
Journal of Mathematical Imaging and Vision 20: 251–265, 2004

Isotropic Energies, Filters and Splines for Vector Field Regularization

PASCAL CACHIER* AND NICHOLAS AYACHE
Epidaure Lab, INRIA-Sophia, 2004 route des lucioles, 06902 Sophia Antipolis Cedex, France
pascal.cathier@siemens.com
nicholas.ayache@sophia.inria.fr

Abstract. The aim of this paper is to propose new regularization and filtering techniques for dense and sparse vector fields, and to focus on their application to non-rigid registration. Indeed, most of the regularization energies used in non-rigid registration operate independently on each coordinate of the transformation. The only common exception is the linear elastic energy, which enables cross-effects between coordinates. Cross-effects are yet essential to give realistic deformations in the uniform parts of the image, where displacements are interpolated.

In this paper, we propose to find isotropic quadratic differential forms operating on a vector field, using a known theorem on isotropic tensors, and we give results for differentials of order 1 and 2. The quadratic approximation induced by these energies yields a new class of vectorial filters, applied numerically in the Fourier domain. We also propose a class of separable isotropic filters generalizing Gaussian filtering to vector fields, which enables fast smoothing in the spatial domain. Then we deduce splines in the context of interpolation or approximation of sparse displacements. These splines generalize scalar Laplacian splines, such as thin-plate splines, to vector interpolation. Finally, we propose to solve the problem of approximating a dense and a sparse displacement field at the same time. This last formulation enables us to introduce sparse geometrical constraints in intensity based non-rigid registration algorithms, illustrated here on intersubject brain registration.

Keywords: vector field regularization, non-rigid registration, convolution filter, spline

1. Introduction

The goal of this paper is to propose new regularization and filtering techniques for dense or sparse vector fields. Although the scope of this study is general, we focus here more precisely on its application to non-rigid registration. Non-rigid registration is a fundamental task of image processing, which consists in deforming one image into the geometry of the other, so that similar structures correspond. Non-rigid registration is used e.g. for pattern recognition, object tracking, image sequence compression, and in the medical area, for atlas generation or matching and for follow-up studies.

There are two main non-rigid registration methods. The first one is the geometric feature based approach. Some geometric features, such as points, lines or surfaces, are extracted beforehand in the images; then, a geometric distance D is used to match these two sets. The second one is the intensity-based approach. An intensity similarity is used as a distance D between the images. Points are moved so that this similarity increases.

In both cases, it is not sufficient to rely only on geometric or intensity features, because this does not ensure any spatial correlation between the displacement of close points. Spatial correlation is a strong a priori knowledge that enables a much better estimation of the displacement. In the case of the geometric feature approach, spatial correlation should also give the possibility to extrapolate the displacement to non-segmented points. One has thus to choose a *motion model* to enforce this continuity constraint—which besides may allow occasional discontinuities.

*Now with Siemens Medical Solutions, Malvern, PA, USA.

This paper focuses on motion models based on a regularization energy R (also sometimes called stabilizer), that is minimized in a weighted sum with the distance D. Interestingly, this regularization energy can be related to a prior probability distribution on the transformation that depends on its smoothness [23]. When this energy is quadratic, convolutions filters and splines can be deduced for regularizing resp. dense and sparse vector fields.

Most of the time, this regularization energy is simply a sum of energies depending on one coordinate of the transformation, e.g. $R(\mathbf{f}) = r(f_x) + r(f_y)$ in 2D. Practically, this means that the filters or splines mentioned above are scalar and applied to each coordinate independently. However, this does not let the possibility of coupling coordinates, which is yet essential to yield realistic motions: in a real material, a constraint along an axis would also affect the position of points along the other axes.

A common exception is the linear elastic energy, used since long in non-rigid registration [2]. This is the kind of energy we are interested in, since its two parameters enable to control both the regularization strength and the coupling between coordinates. However the linear elastic energy is not satisfactory for at least two reasons: firstly, the impulse response of its associated convolution filter has a very strong discontinuity in its derivative, which may yield quite unsmooth regularized fields; secondly, there is not spline associated to this energy, even if substitutes have been designed [8], so this energy cannot be used for point landmark registration.

In this paper, we propose to find vector field regularization energies. We will restrict ourselves to *differential quadratic forms* (DQF), with the additional constraint that they should be *isotropic*, i.e. invariant by rotation and mirror symmetry. This might sound restrictive. However, isotropic DQFs are often used as is for fast regularization. Furthermore, more complex regularization techniques are often based on isotropic DQFs—for example, one can easily introduce anisotropy [1], non-uniformly weights [24], M-estimators [12], a Mumford-Shah formulation [25], etc., to obtain more complex, non-quadratic regularization energies.

There has been few papers going in that direction. The work closest to ours has been done by Gabrani [11]. In this framework, motion fields are derived as being the gradient of a scalar functionnal (Airy's stress function), on which the regularization energy actually holds. The authors are then able to derive splines with explicit formulas for point-landmark registration. Another related work has been done by Davis et al. [8], where the autors attempt to extend the work of Duchon [10] to linear elasticity.

It is worth noting that our goal is quite different from general vector image regularization, e.g. for color images—see for example [3, 7, 15, 21]. Conceptually, the main problem for vector image regularization is not how to propagate the value of vectors (intuitively, the same value will be propagated with a weight decreasing with distance), but to which extent to propagate them according to the local structure of the image. The main problem addressed by these techniques is thus how to extract structure information for "edge preserving", non-linear smoothing.

In our case, we work with vector fields, for which vectors have exactly the same dimension as the image. Our problem is not a particular case of the previous one, but an orthogonal one: it really addresses the question of how to propagate the displacement of a point to its neighbors. The propagated value is not necessarily a rescaling of the original value: coordinates may be combined, leading to rotation of the vector. By contrast, if one has to smooth a red object on a black background, creation of other colors such as blue or green is generally not desirable. The work proposed here is therefore not applicable to general vector image regularization if vectors do not carry a motion-like information. However, one could extend the work introduced here to non-linear regularization using techniques similar to the previous papers.

In Section 2, we propose to find all possible isotropic differential quadratic forms (IDQFs) of vector fields using a known theorem on isotropic tensors, and apply it to IDQFs of order 1 and 2.

In Section 3, we deduce vector convolution filters from the previous IDQFs. Contrary to conventional scalar filters, these vector filters allow cross-effects between coordinates, yielding more realistic displacements. We also give a set of fast, separable filters that generalizes Gaussian filtering to vectors.

Similarly, in Section 4, we deduce splines from IDQFs. Again, contrary to conventional scalar splines or radial basis functions, these vectorial splines allow cross-effects between coordinates. These splines generalize Laplacian splines such as the thin plate spline.

In Section 5, we finally propose to merge dense and sparse approximation problems, and show that their solutions are linear combinations of filters and splines. This regularization technique turns out to be

extremely useful for introducing geometrical landmarks in intensity-based registration algorithm, which is illustrated in this paper on intersubject brain registration.

2. Isotropic Differential Quadratic Forms (IDQF)

In this section, we aim at finding differential quadratic forms (DQF) that are isotropic. DQFs are sums of products of two partial derivatives of a vector field; therefore, their number increases exponentially with the space dimension and with the differential order. However, only a small number of them are isotropic. A theorem on isotropic tensors helps us to find them.

2.1. Mathematical Definitions and Notations

We note $\mathbb{R}^d$ the real vector space of dimension d, $\mathcal{M}(d)$ the group of linear functions of $\mathbb{R}^d$ in itself, and $O(d) \in \mathcal{M}(d)$ its subgroup composed of orthogonal functions R, such that $R^T R = RR^T = \mathrm{Id}_d$. Also, to avoid long mathematical expressions, we use in the following a simplified[1] Einstein summation convention, for which every index repeated twice in a product is implicitly summed all over its range.

Definition 1 (Tensor). A tensor T of order $n \geq 1$ in a space of dimension $d \geq 1$ has d^n components, noted $T_{i_1 i_2 \ldots i_n}$, $i_k \in [\![1; d]\!]$, $\forall k \in [\![1; n]\!]$, which transform under the action of $A = (a_{ij}) \in \mathcal{M}(d)$ in the following way: if $A \star T$ is the resulting tensor, then

$$A \star T_{i_1 \ldots i_n} = a_{i_1 j_1} \ldots a_{i_n j_n} T_{j_1 \ldots j_n}$$

We note $\mathcal{T}(n, d)$ the set of these tensors.

Definition 2 (Differential tensor). The partial derivatives $\partial_{i_1 \ldots i_n} f_{i_{n+1}}$ of a vector field $\mathbf{f}$ of dimension d form a tensor of $\mathcal{T}(n+1, d)$ called the n-th order differential tensor of $\mathbf{f}$.

Definition 3 (Quadratic form of tensors). We note $\mathcal{Q}(n, d)$ the set of quadratic form of tensors $T \in \mathcal{T}(n, d)$, which can be represented by d^{2n} numbers $q_{i_1 \ldots i_n j_1 \ldots j_n}$, $(i_k, j_k) \in [\![1; d]\!]^2$, $\forall k \in [\![1; n]\!]$, so that

$$q(T) = q_{i_1 \ldots i_n j_1 \ldots j_n} T_{i_1 \ldots i_n} T_{j_1 \ldots j_n}$$

with $q_{i_1 \ldots i_n j_1 \ldots j_n} = q_{j_1 \ldots j_n i_1 \ldots i_n}$.

Property 1. *If $q \in \mathcal{Q}(n, d)$, $T \in \mathcal{T}(n, d)$ and $A \in \mathcal{M}(d)$,*

$$q(A \star T) = q_{i_1 \ldots i_n j_1 \ldots j_n} a_{i_1 k_1} \ldots a_{i_n k_n} a_{j_1 l_1} \ldots a_{j_n l_n} T_{k_1 \ldots k_n} T_{l_1 \ldots l_n}$$

The $q_{i_1 \ldots i_n j_1 \ldots j_n}$ therefore form a tensor of order $2n$.

2.2. Isotropy

Definition 4 (Isotropic tensors). A tensor $T \in \mathcal{T}(n, d)$ is isotropic if it is invariant by an orthogonal change of the tensor, i.e. if for any orthogonal function $R = (r_{ij}) \in O(d)$,

$$R \star T = T$$

or more explicitely, if

$$T_{i_1 \ldots i_n} = r_{i_1 j_1} \ldots r_{i_n j_n} T_{j_1 \ldots j_n} \quad \forall (i_1 \ldots i_n) \in [\![1; d]\!]^n$$

Definition 5 (IDQF). Isotropic quadratic forms of the n-th order differential tensor of a vector field are called isotropic differential quadratic forms (IDQFs). Their coefficients form an isotropic tensor of order $2n + 2$.

Theorem 1 (*Isotropic tensors*). *An isotropic tensor of order n, n even, can be written as a linear combination of the $n!/(2^{n/2}(n/2)!)$ products of Kronecker tensors $\delta_{i_r i_s}$. The only isotropic tensor of order n, n odd, is the null tensor.*

The demonstration of this result can be found in [13, 26].

2.3. First Order IDQFs

According to Theorem 1, an isotropic tensor of order 4 is a linear combination of the three following tensors:

$$\delta_{i_1 i_2} \delta_{i_3 i_4} \quad \delta_{i_1 i_3} \delta_{i_2 i_4} \quad \delta_{i_1 i_4} \delta_{i_2 i_3}$$

Therefore, a first order IDQF q, which can be seen as a tensor of order 4, is a linear combination of the tensors $\partial_i f_i \partial_j f_j$, $\partial_i f_j \partial_i f_j$ and $\partial_i f_j \partial_j f_i$.

Property 2. *For any IDQF q of the first derivative of a vector field* $\mathbf{f}$*, we can find three coefficients* a_1, a_2, a_3 *so that*

$$q(\mathbf{f}) = a_1 \cdot \mathrm{tr}(\nabla \mathbf{f}^T \nabla \mathbf{f}) + a_2 \cdot \mathrm{tr}(\nabla \mathbf{f} \nabla \mathbf{f}) + a_3 \cdot \mathrm{tr}^2(\nabla \mathbf{f}) \tag{1}$$

with $\mathrm{tr}(\nabla \mathbf{f}^T \nabla \mathbf{f}) = \partial_i f_j \partial_i f_j$, $\mathrm{tr}(\nabla \mathbf{f} \nabla \mathbf{f}) = \partial_i f_j \partial_j f_i$ *and* $\mathrm{tr}^2(\nabla \mathbf{f}) = \partial_i f_i \partial_j f_j$

Linear elasticity is the particular case where $a_1 = \lambda/2$ and $a_2 = a_3 = \mu/2$, where λ and μ are Lamé coefficients.

2.4. Positive First Order IDQFs

A quadratic regularization energy should be positive, in order to penalize non-smooth estimations. Therefore, one should find the conditions on a_1, a_2 and a_3 under which the IDQF remains positive for any set of partial derivatives.

The linear function $Q : \mathcal{M}_n \to \mathcal{M}_n$ associated to q given by Eq. (1) is defined by:

$$Q(M) = a_1 M_{i,j} \cdot E^{(i,j)} + a_2 M_{i,j} E^{(j,i)} + a_3 M_{i,i} E^{(j,j)}$$

where $E^{(i,j)}$ is the matrix of $\mathcal{M}_n$ whose only non-zero element is $E^{(i,j)}_{i,j} = 1$. Its eigenmatrices are reported in the following array:

Eigenmatrix	Eigenvalue
Id	$a_1 + a_2 + d a_3$
$E^{(i,j)} + E^{(j,i)}, (i,j) \in [\![1;d]\!]^2, i \neq j$	$a_1 + a_2$
$E^{(i,j)} - E^{(j,i)}, (i,j) \in [\![1;d]\!]^2, i \neq j$	$a_1 - a_2$
$F_i, i \in [\![2;d]\!]$	$a_1 + a_2$

where $F_1 = \mathrm{Id}$ and $(F_1, \ldots, F_d)$ is an orthogonal basis of the space generated by the set $\{E^{(i,i)}, i \in [\![1;d]\!]\}$. All these eigenmatrices are orthogonal, and we have exactly $1 + d(d-1)/2 + d(d-1)/2 + (d-1) = d^2$ of them, so there does not exist any other eigenvalue than the three listed above.

Therefore, a first order IDQF q is positive if we simultaneously have $a_1 + a_2 \geq 0$, $a_1 - a_2 \geq 0$ and $a_1 + a_2 + d a_3 \geq 0$.

2.5. Second Order IDQFs

According to Theorem 1, an isotropic tensor of order 6 is a linear combination of products of Kronecker tensors of the form $\delta_{i_r i_s} \delta_{i_t i_u} \delta_{i_v i_w}$. There are 15 such tensors.

This set of generators can nonetheless be reduced. First, it is known that the isotropic tensors given by Theorem 1 are not independent. A minimal, independent set of isotropic tensors that generates all isotropic tensors by linear combination can be found for example in [22]. Second, the quadratic forms we are interested in are tensors with specific symmetries, due to the commutation of multiplication and differentiation assumed here: this also reduces the number of functions necessary to generate second order isotropic quadratic energies. This is done in Appendix A, and leads to the following result:

Property 3. *For any second order IDQF of a vector field* $\mathbf{f}$*, we can find five coefficients* a_1, a_2, a_3, a_4, a_5 *so that*

$$q(\mathbf{f}) = a_1 Q_1(\mathbf{f}) + a_2 Q_2(\mathbf{f}) + a_3 Q_3(\mathbf{f}) + a_4 Q_4(\mathbf{f}) + a_5 Q_5(\mathbf{f})$$

with $Q_1(\mathbf{f}) = \partial_{ij} f_k \partial_{ij} f_k$, $Q_2(\mathbf{f}) = \partial_{ij} f_j \partial_{ik} f_k$, $Q_3(\mathbf{f}) = \partial_{ii} f_j \partial_{kk} f_j$, $Q_4(\mathbf{f}) = \partial_{ij} f_k \partial_{kj} f_i$ *and* $Q_5(\mathbf{f}) = \partial_{ii} f_j \partial_{kj} f_k$.

2.6. Conclusion

Theorem 1 is convenient to find IDQFs almost automatically. However, this set being non linearly independent, one may want to reduce it; this task is less trivial because of the special symmetries of IDQFs. Furthermore, apart from first order IDQFs, it is also not trivial to compute conditions of positiveness on the IDQF coefficients, which are yet essential for regularization purposes. However, as shown in next sections, one can overcome these problems by dealing directly with the filters or splines associated with these energies.

3. Isotropic Convolution Filters for Vector Fields

Filters can be deduced from quadratic regularization energies R by looking at the closed-form solution of the homogeneous dense approximation problem, which consists in approximating a possibly noisy vector field

$\mathbf{g}$ by a smooth vector field $\mathbf{f}$ by minimizing the energy

$$E(\mathbf{f}) = \int \|\mathbf{f} - \mathbf{g}\|^2 + R(\mathbf{f}) \qquad (2)$$

Solving this problem in the Fourier space, we obtain a closed form equation for f

$$\hat{f} = M^{-1}\hat{g}$$

where $\hat{}$ denotes the Fourier transform, and M^{-1} is a $d \times d$ symmetric matrix which is the Fourier transform of the convolution filter we are looking for.

3.1. First Order Isotropic Filters

3.1.1. Functional Derivatives of First Order IDQFs. The functional derivatives w.r.t. $\mathbf{f}$ of the generating elements of first order IDQFs given by Property 2 are reported in the following array.

Quadratic form		Derivative
$\partial_i f_j \partial_i f_j$	$\longrightarrow$	$-2\Delta\mathbf{f}$
$\partial_i f_j \partial_j f_i$	$\longrightarrow$	$-2\nabla\nabla^T\mathbf{f}$
$\partial_i f_i \partial_j f_j$	$\longrightarrow$	$-2\nabla\nabla^T\mathbf{f}$

where Δ denotes the Laplacian. Now, the differentiation of the approximation energy (2) w.r.t $\mathbf{f}$, when R is a first order IDQF given by (1), yields

$$\alpha\Delta\mathbf{f} + \beta\nabla\nabla^T\mathbf{f} = \mathbf{g} - \mathbf{f} \qquad (3)$$

with $\alpha = a_1$ and $\beta = a_2 + da_3$. This equation (3) corresponds to a linear elastic PDE, with external forces $\mathbf{g} - \mathbf{f}$ corresponding to linear springs attracting $\mathbf{f}$ towards $\mathbf{g}$. According to Section 2.4, we should choose a_1, a_2 and a_3 so that $a_1 + a_2 \geq 0$, $a_1 - a_2 \geq 0$ and $a_1 + a_2 + da_3 \geq 0$. Combining these inequalities, we find that $\alpha \geq 0$ and $\beta \geq -\alpha$.

3.1.2. On the Number of Degrees of Freedom. It appears that two out of the three generating IDQFs have the same functional derivatives. Therefore, here we have only two degrees of freedom (corresponding to α and β) to shape the regularization process.

This situation is similar to the scalar case, for which there exist several isotropic quadratic regularization energies at any order of derivation, but all of them having the same derivatives [17]. Brady and Horn [4] showed that boundary conditions are critical to tell these energies apart: they potentially contain the other DOF.

When using Fourier transform, the implicit boundary conditions are periodicity, i.e. we consider that opposite image borders are connected. With these assumptions, there is no other degree of freedom that those given by the derivative.

3.1.3. Resolution in the Fourier Domain. The linear differential equation (3) can be solved in the Fourier space. We have the following equivalence between spatial and Fourier domains:

Spatial domain		Fourier domain
$\Delta\mathbf{f}(\mathbf{x})$	$\longleftrightarrow$	$-(\mathbf{w}^T\mathbf{w})\hat{\mathbf{f}}(\mathbf{w})$
$(\nabla\nabla^T)\mathbf{f}(\mathbf{x})$	$\longleftrightarrow$	$-(\mathbf{w}\mathbf{w}^T)\hat{\mathbf{f}}(\mathbf{w})$

where $\mathbf{x} = (x_1, \ldots, x_d)$ and $\mathbf{w} = (w_1, \ldots, w_d)$ are the canonical coordinates of resp. the spatial and the Fourier domain. Equation (3) transforms in the Fourier domain as:

$$\underbrace{[(1 + \alpha\mathbf{w}^T\mathbf{w})\mathrm{Id} + \beta\mathbf{w}\mathbf{w}^T]}_{M_1}\hat{\mathbf{f}} = \hat{\mathbf{g}}$$

For homogeneity reasons explained in Section 3.3.3, we replace the parameters α and β by $\alpha = \lambda$ and $\beta = \lambda\kappa$, so that λ can be identified to a regularization strength and κ to a cross-effect strength; positiveness conditions become $\lambda \geq 0$ and $\kappa \geq -1$. We invert M_1 to solve the previous equation:

$$M_1^{-1} = \frac{1}{1 + \lambda\mathbf{w}^T\mathbf{w}}\left[\mathrm{Id} - \frac{\lambda\kappa}{1 + \lambda(1+\kappa)\mathbf{w}^T\mathbf{w}}\mathbf{w}\mathbf{w}^T\right] \qquad (4)$$

Now, to fit $\mathbf{f}$ to $\mathbf{g}$ with the approximation energy (2) where R is a first order IDQF, we proceed in three steps: (1), compute the Fourier transform of $\mathbf{g}$; (2), multiply this Fourier transform by Eq. (4); (3), compute the inverse Fourier transform of this product, yielding the solution.

3.1.4. Impulse Response. We show three examples of first order isotropic filters, depending on the sign of the cross-effect parameter κ, which acts as the Poisson ratio ν of the theory of elasticity. Here, the vector field $\mathbf{g}$ to be smoothed is a simple impulse along the horizontal axis (Fig. 1). The results shown in Fig. 2 can be considered as the impulse response of their respective filter.

The first filter, Fig. 2(a), does not present any cross-effect ($\kappa = 0$) and corresponds to a membrane model. Without cross effects, horizontal lines stay straight: there is no motion along the vertical axis because the input impulse itself has no vertical component.

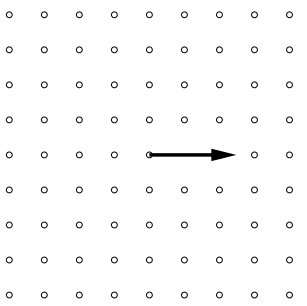

Figure 1. Impulse responses are obtained here by applying filters to this vector field, which is null except for the central point which is moved to the right.

The second filter, Fig. 2(b), presents cross-effects ($\kappa > 0$); the tissue gets closer to an incompressible model and the material is less deformed: this can be interesting for registration purposes, for example if the organs to be registered are nearly incompressible, such as the brain.

The last filter, Fig. 2(c), also has cross-effects ($\kappa < 0$), but its behavior is somewhat counter-intuitive as the impulse tends to inflate the material behind it. Although some rare materials do have this kind of behavior, e.g. foams with negative Poisson ratio [16], the choice of a negative κ for registration has more to do with a prior knowledge on the displacement (e.g. inflations or contractions).

For any value of λ or κ, there exists a discontinuity in the derivative of the impulse response, at the tip of the sharp peak. In non-rigid registration, external forces are dense, and applied at every pixel of the image, therefore such peaks may appear frequently in the image. This is particularly annoying if a further processing uses a differential analysis of the computed displacement field, e.g. a Jacobian based segmentation as in [18]. For this purpose, we need filters of order higher than these linear elastic filters.

3.1.5. Isotropy vs. Rotation Invariance. As a remark, let us highlight that the symmetry invariance is essential, and that rotation invariance alone, which is sufficient in the scalar case [4, 17], is not sufficient anymore in the vectorial case.

In Fig. 3, we give the impulse response of a first order rotation invariant but non-isotropic filter. The rotation invariance ensures that if the initial impulse is rotated, then the impulse response is rotated by the same amount. The symmetry invariance would ensure a planar symmetry of the impulse response; without this constraint, the impulse response may bend on either side, as if the material was undergoing an internal torsion. These kind of effects are generally not desirable.

3.2. Second Order Isotropic Filters

3.2.1. Functional Derivatives of Second Order IDQFs. We follow the same strategy and begin by differentiating the basis of second order IDQF:

Quadratic form	Derivative
$\partial_{ij}\mathbf{f}_k \partial_{ij}\mathbf{f}_k$	$\longrightarrow 2\Delta^2\mathbf{f}$
$\partial_{ij}\mathbf{f}_j \partial_{ik}\mathbf{f}_k$	$\longrightarrow 2\Delta\nabla\nabla^T\mathbf{f}$
$\partial_{ii}\mathbf{f}_j \partial_{kk}\mathbf{f}_j$	$\longrightarrow 2\Delta^2\mathbf{f}$
$\partial_{ij}\mathbf{f}_k \partial_{kj}\mathbf{f}_i$	$\longrightarrow 2\Delta\nabla\nabla^T\mathbf{f}$
$\partial_{ii}\mathbf{f}_j \partial_{kj}\mathbf{f}_k$	$\longrightarrow 2\Delta\nabla\nabla^T\mathbf{f}$

So the functional derivative of Eq. (2), where now R is a second order IDQF, is

$$\alpha\Delta^2\mathbf{f} + \beta\Delta\nabla\nabla^T\mathbf{f} = \mathbf{f} - \mathbf{g} \tag{5}$$

Although we did not characterized positive second order IDQFs, we can ensure a proper regularization by finding a particular IDQF whose functional derivative

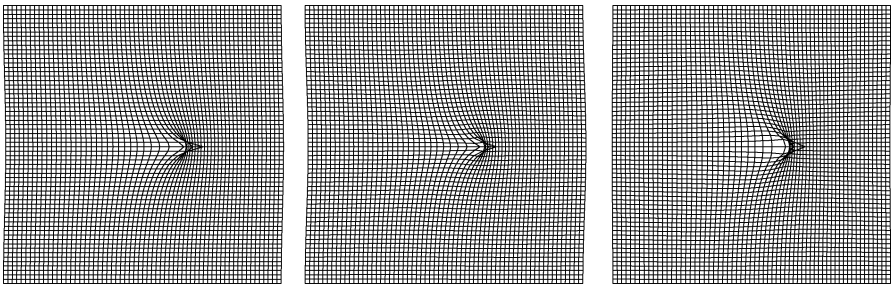

Figure 2. Impulse response of three different first order isotropic filters.

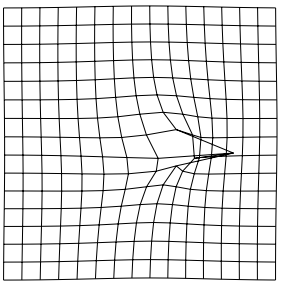

Figure 3. Impulse response of a rotation-invariant but non-isotropic filter.

yields Eq. (5), and whose positiveness conditions are simpler to compute than in the general case. Indeed, the left member of (5) is (proportional to) the derivative of the second order IDQF $\alpha\partial_{ij} f_k \partial_{ij} f_k + \beta \partial_{ij} f_k \partial_{kj} f_i$, whose related linear function is

$$Q(T_{i,j,k}) = \alpha T_{i,j,k} E^{(i,j,k)} + \beta T_{i,j,k} E^{(i,j,k)}$$

where $E^{(i,j,k)}$ is the tensor whose single non-zero element is $E^{(i,j,k)}_{i,j,k} = 1$. The eigentensors and eigenvalues of this linear function are

Eigentensor	Eigenvalue
$E^{(i,j,k)} - E^{(k,j,i)}, \forall (i,j,k) \in [\![1;d]\!]^3, i > k$	$\alpha - \beta$
$E^{(i,j,k)} + E^{(k,j,i)}, \forall (i,j,k) \in [\![1;d]\!]^3, i > k$	$\alpha + \beta$
$E^{(i,j,k)}, \forall (i,j) \in [\![1;d]\!]^2$	$\alpha + \beta$

There are $d^2(d-1)/2 + d^2 + d^2(d-1)/2 = d^3$ such eigenvectors, which are orthogonal, therefore there is no any other eigenvalue.

Thus, the quadratic form is positive if $\alpha + \beta \geq 0$ and $\alpha - \beta \geq 0$, i.e. if $\alpha \geq 0$ and $\beta \geq -\alpha$. These are exactly the same conditions as in the first order case.

3.2.2. Resolution in the Fourier Domain. We have the following correspondences between the spatial domain and the Fourier domain:

Spatial domain	Fourier domain
$\Delta^2 \mathbf{f}(\mathbf{x})$	$\longleftrightarrow (\mathbf{w}^T\mathbf{w})^2 \hat{\mathbf{f}}(\mathbf{w})$
$\Delta\nabla\nabla^T \mathbf{f}(\mathbf{x})$	$\longleftrightarrow \mathbf{w}^T\mathbf{w}(\mathbf{w}\mathbf{w}^T)\hat{\mathbf{f}}(\mathbf{w})$

Thus, in the Fourier domain, the differential equation (5) becomes:

$$\underbrace{[(1+\lambda(\mathbf{w}^T\mathbf{w})^2)\mathrm{Id} + \lambda\kappa(\mathbf{w}^T\mathbf{w})(\mathbf{w}\mathbf{w}^T)]}_{M_2}\hat{\mathbf{f}} = \hat{\mathbf{g}}$$

with $\lambda = \alpha \geq 0$ and $\kappa = \beta/\alpha \geq -1$. We now invert M_2, yielding:

$$M_2^{-1} = \frac{1}{1+\lambda(\mathbf{w}^T\mathbf{w})^2}\left[\mathrm{Id} - \frac{\lambda\kappa}{1+\lambda(1+\kappa)(\mathbf{w}^T\mathbf{w})^2}\mathbf{w}\mathbf{w}^T\right]$$

This leads to an implementation identical to the first order case, Section 3.1.3.

3.2.3. Impulse Response. In Fig. 4, we present the impulse response of the second order filter for three different values of κ, one without any cross-effect ($\kappa = 0$) corresponding to a thin-plate model, and two others with positive and negative cross-effects. The impact of κ on the filter is similar as in the first order case, i.e. that of a Poisson ratio. However, impulse responses are much smoother, which makes differential analysis and one-to-one mapping easier to achieve in practice.

3.3. Generalization

3.3.1. Higher-Order Isotropic Filters. Given the results obtained for first and second order isotropic regularization energies, we are tempted to generalize the linear PDE to higher order regularization. Even though we did not characterize the n-th order IDQFs, we can set the PDE for the n-th order regularization as:

$$(-1)^n[\alpha\Delta^n\mathbf{f} + \beta\Delta^{n-1}\nabla\nabla^T\mathbf{f}] = \mathbf{f} - \mathbf{g}$$

which is indeed isotropic, since it is related to the functional derivative of the following isotropic quadratic form:

$$\begin{aligned} E_n(\mathbf{f}) = {} & \alpha \cdot \partial_{i_1\ldots i_n} f_{i_{n+1}} \partial_{i_1\ldots i_n} f_{i_{n+1}} \\ & + \beta \cdot \partial_{i_1\ldots i_n} f_{i_{n+1}} \partial_{i_{n+1} i_2 \ldots i_n} f_{i_1} \end{aligned} \quad (6)$$

The linear function associated to this quadratic form is

$$Q(T) = \alpha T_{i_1,\ldots i_{n+1}} E^{(i_1,\ldots i_{n+1})} + \beta T_{i_1,\ldots i_{n+1}} E^{(i_{n+1},i_2,\ldots i_n,i_1)}$$

where $E^{(i_1,\ldots i_{n+1})}$ is the tensor whose only non-zero element is $E^{(i_1,\ldots i_{n+1})}_{i_1,\ldots i_{n+1}} = 1$. Its eigentensors and associated

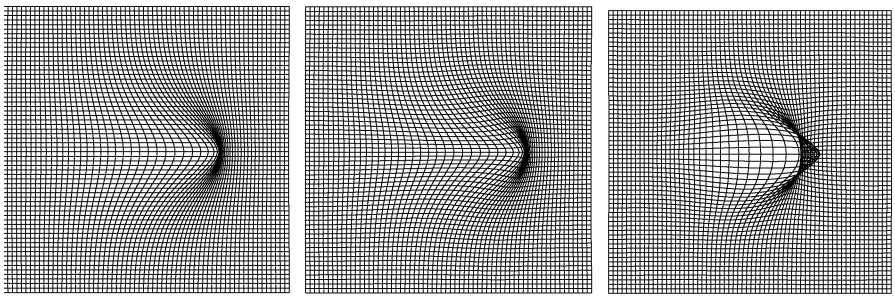

Figure 4. Impulse response of three different second order isotropic filters.

eigenvalues are:

Eigentensor	Eigenvalue
$E^{(i_1,\ldots i_{n+1})} + E^{(i_{n+1},i_2,\ldots i_n,i_1)}, i_1 \ldots i_{n+1}$ $\in [\![1;d]\!], i_1 > i_{n+1}$	$\alpha+\beta$
$E^{(i_1,\ldots i_{n+1})} - E^{(i_{n+1},i_2,\ldots i_n,i_1)}, i_1 \ldots i_{n+1}$ $\in [\![1;d]\!], i_1 > i_{n+1}$	$\alpha-\beta$
$E^{(k,i_2,\ldots i_n,k)}, k, i_2, \ldots, i_n \in [\![1;d]\!]$	$\alpha-\beta$

All these d^n tensors are orthogonal. Therefore, there exists no additional eigenvalue, and as for the first and second order regularization, positiveness conditions are $\alpha \geq 0$ and $\beta \geq -\alpha$.

We have the following correspondences between the spatial domain and the Fourier domain:

Spatial domain	Fourier domain
$\Delta^n \mathbf{f}(\mathbf{x})$	$\longleftrightarrow (-1)^n(\mathbf{w}^T\mathbf{w})^n\hat{\mathbf{f}}(\mathbf{w})$
$\Delta^{n-1}(\nabla\nabla^T)\mathbf{f}(\mathbf{x})$	$\longleftrightarrow (-1)^n(\mathbf{w}^T\mathbf{w})^{n-1}(\mathbf{w}\mathbf{w}^T)\hat{\mathbf{f}}(\mathbf{w})$

The differential equation becomes (setting $\alpha = \lambda$ and $\beta = \lambda\kappa$):

$$\underbrace{[(1+\lambda(\mathbf{w}^T\mathbf{w})^n)\mathrm{Id} + \lambda\kappa(\mathbf{w}^T\mathbf{w})^{n-1}(\mathbf{w}\mathbf{w}^T)]}_{M_n}\hat{\mathbf{f}} = \hat{\mathbf{g}}$$

To solve this equation, we invert the matrix M_n:

$$M_n^{-1} = \frac{1}{1+\lambda(\mathbf{w}^T\mathbf{w})^n} \times \left[\mathrm{Id} - \frac{\lambda\kappa}{1+\lambda(1+\kappa)(\mathbf{w}^T\mathbf{w})^n}\mathbf{w}\mathbf{w}^T\right] \quad (7)$$

3.3.2. Multi-Order Filters. A regularization energy may include several or even all orders of derivation. Let us consider linear combinations of energies (6)

$$\sum_{n=1}^{\infty} \alpha_n \partial_{i_1\ldots i_n} f_{i_{n+1}} \partial_{i_1\ldots i_n} f_{i_{n+1}} + \beta_n \partial_{i_1\ldots i_n} f_{i_{n+1}} \partial_{i_{n+1} i_2\ldots i_n} f_{i_1} \quad (8)$$

The associated regularization PDE is

$$\sum_{n=1}^{\infty}(-1)^n[\alpha_n\Delta^n\mathbf{f} + \beta_n\Delta^{n-1}\nabla\nabla^T\mathbf{f}] = \mathbf{f}-\mathbf{g}$$

with two scalar $\alpha_n \geq 0$ and $\beta_n \geq -\alpha_n$ to choose per order of derivation, corresponding approximately to its strength and its shear. In the Fourier domain, the previous PDE becomes

$$\underbrace{\left[\left(1+\sum_{n=1}^{\infty}\alpha_n(\mathbf{w}^T\mathbf{w})^n\right)\mathrm{Id} + \sum_{n=1}^{\infty}\beta_n(\mathbf{w}^T\mathbf{w})^{n-1}(\mathbf{w}\mathbf{w}^T)\right]}_{M} \times \hat{\mathbf{f}} = \hat{\mathbf{g}}$$

As previously, one should invert matrix M and apply it to the Fourier transform of $\mathbf{g}$ to obtain the solution.

3.3.3. A Note on the Regularization Strength. Energies (8) are designed for regularization. Therefore, we should be able to control their weight relatively to another energy, e.g. an intensity similarity measure, *via* a regularization parameter λ.

In the case of quadratic approximation, choosing λ as a global multiplicative factor, $\lambda R(\mathbf{f})$, gives counterintuitive results, because λ changes the shape of the impulse response instead of just rescaling it. If we want a regularization strength λ that corresponds to a scale

factor of the impulse response, as for Gaussian filters, we have to put it inside the energy

$$R(\mathbf{f},\lambda)=\sum_{n=1}^{\infty}\lambda^n\big[\alpha_n\partial_{i_1\dots i_n}f_{i_{n+1}}\partial_{i_1\dots i_n}f_{i_{n+1}} + \beta_n\partial_{i_1\dots i_n}f_{i_{n+1}}\partial_{i_{n+1}i_2\dots i_n}f_{i_1}\big]$$

Now λ is a parameter of the regularization energy. Of course, if the regularization energy uses only one order of differentiation, which is quite frequent in non-rigid registration, both approaches are equivalent.

3.4. Separable Isotropic Filters

Previous vectorial convolution filters are applied in the Fourier domain—this is indeed generally the faster way to proceed, especially in 3D and for large kernels. However, the computation can be even faster in the real domain, if the kernel is separable.

3.4.1. Definitions

Definition 6 (Isotropic filters). A scalar convolution kernel $f(\mathbf{x}):\mathbb{R}^d\to\mathbb{R}$ is isotropic if $f(R^T\mathbf{x})=f(\mathbf{x})$, $\forall R\in O(d)$. A vector convolution kernel $F(\mathbf{x})=F(x_1,\dots,x_d):\mathbb{R}^d\to\mathcal{M}_d$ is isotropic if $RF(R^T\mathbf{x})R^T=F(\mathbf{x}),\forall R\in O(d)$.

Definition 7 (Separable filters). A scalar convolution kernel $f(\mathbf{x})=f(x_1,\dots,x_d):\mathbb{R}^d\to\mathbb{R}$ is separable if there exists d functions $f_k, k\in[\![1;d]\!]$, such that $f(\mathbf{x})=f_1(x_1)f_2(x_2)\dots f_d(x_d)=\prod_{k=1}^d f_k(x_k)$. A vector convolution kernel $F(\mathbf{x})=F(x_1,\dots,x_d):\mathbb{R}^d\to\mathcal{M}_d$ is separable if each of its element $F_{i,j}$ is separable.

Note that there are other possible definitions of separability for vectorial filters. The property of separability is very interesting from a numerical point of view, because n-dimensional convolutions then boil down to a sequence of 1-D convolutions, which can be implemented efficiently for instance using recursive filtering.

The choice of separable filters is drastically reduced if we also impose the isotropy property. For scalars, it is known that the only isotropic separable kernels are the family of Gaussians [14]. However, to the best of our knowledge, there is no similar theorem for vector filters. We propose the following result, easy to verify:

Proposition 1. *The vector filter $G_{\sigma,\kappa}$ defined by*

$$G_{\sigma,\kappa}(\mathbf{x})=\frac{1}{(\sigma\sqrt{2\pi})^d(1+\kappa)}\left(\mathrm{Id}_d+\frac{\kappa}{\sigma^2}\mathbf{x}\mathbf{x}^T\right)e^{-\frac{\mathbf{x}^T\mathbf{x}}{2\sigma^2}} \tag{9}$$

is separable and isotropic.

The normalization coefficient $(\sigma\sqrt{2\pi})^d(1+\kappa)$ is chosen so that a constant vector field is unchanged by convolution with $G_{\sigma,\kappa}$. As previously, the coefficient κ act as a Poisson ratio. When κ is set to zero, the matrix $G_{\sigma,0}$ is diagonal and we obtain a classical Gaussian filtering, independently on each component of the vector field.

There exist separable isotropic filters that are not part of this previous family, as this filter in 2D:

$$\frac{1}{(\sigma\sqrt{2\pi})^2(1-\kappa)}\begin{pmatrix}1-\kappa y^2/\sigma^2 & \kappa xy/\sigma^2\\ \kappa xy/\sigma^2 & 1-\kappa x^2/\sigma^2\end{pmatrix}\cdot e^{-\frac{x^2+y^2}{2\sigma^2}}$$

However we could not find counter examples in higher dimension. The filters $G_{\sigma,\kappa}$ given by (5) might be the only separable isotropic filters in dimension greater than or equal to 3, but this has yet to be proven.

3.4.2. Computation with Classical Gaussian Filters

Property 4. *If we note $G_\sigma(\mathbf{x})=\exp(-\mathbf{x}^T\mathbf{x}/(2\sigma^2))/(\sigma\sqrt{2\pi})^d$ the normalized, d-dimensional scalar Gaussian kernel, and $\mathcal{H}G_\sigma$ its Hessian matrix composed of its second order derivatives, the following relation holds*:

$$G_{\sigma,\kappa}(\mathbf{x})=G_\sigma(\mathbf{x})\mathrm{Id}+\frac{\sigma^2\kappa}{1+\kappa}\mathcal{H}G_\sigma(\mathbf{x})$$

Because $G_\sigma(\mathbf{x})\mathrm{Id}$ and $\mathcal{H}G_\sigma(\mathbf{x})$ are also separable, the convolution with $G_{\sigma,\kappa}$ can be computed as a weighted sum of convolutions with a one-dimensional Gaussian, and its first and second derivatives. There exist many efficient techniques to implement these filters—for example Deriche's recursive filters [9], which have a computation time independent of the size of the Gaussian kernel.

3.4.3. Impulse Response. Figure 5 shows the impulse responses of the separable isotropic filter (9) for three different values of parameter κ. Their behavior is somewhat similar to second order filters, Fig. 4, although here the impulse response is even smoother, as the underlying energy is of infinite order.

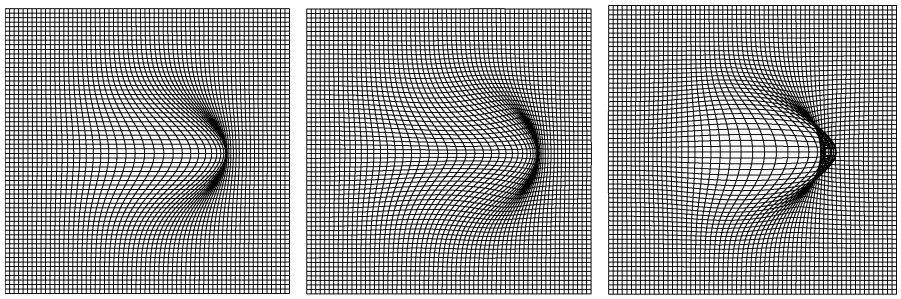

Figure 5. Impulse response of three different separable isotropic vector filters $G_{\sigma,\kappa}$, Eq. (9) generalizing the classical scalar Gaussian filtering to vectors.

3.5. An Application to Image Registration

In the experiment reported in Fig. 6, two circles have been moved apart. They have been registered with PASHA [5], a fast intensity-based non-rigid registration algorithm, using the separable isotropic filters described in Section 3.4, and a simple sum of squared differences as the intensity similarity measure. We ran the algorithm without ($\kappa = 0$) and with cross-effects ($\kappa > 0$).

Without cross-effects, horizontal lines stay horizontal between the circles; there is no noticeable vertical deformation. Choosing $\kappa > 0$ gives a more realistic extrapolation of the displacement, as the material between both circles is bending towards the center. Depending on prior knowledge we have on the material, this latter behavior may be more appropriate.

4. Isotropic Vectorial Splines for Point Matching

In the previous section, quadratic approximation of dense vector fields using isotropic energies gave us a new family of convolution filters. In this section, we now deal with quadratic approximation of sparse vector fields, which yields a new class of splines generalizing Laplacian splines such as the thin plate spline.

4.1. Interpolation and Approximation of Sparse Points

The vector interpolation and approximation problems are a straightforward extension of the scalar ones [10]. Given two sets of points $\mathbf{x}_i$ and $\mathbf{g}_i$ of $\mathbb{R}^d$, the vector interpolation problem consists in finding a vector field $\mathbf{f} : \mathbb{R}^d \to \mathbb{R}^d$ which minimizes a regularization energy $R(\mathbf{f})$ under the constraint that $\mathbf{f}(\mathbf{x}_i) = \mathbf{g}_i$. The vector approximation problem consists in seeking an approximation $\mathbf{f}^*$ which is solution of

$$\mathbf{f}^* = \arg\min_{\mathbf{f}} \sum_i \|\mathbf{g}_i - \mathbf{f}(\mathbf{x}_i)\|^2 + \lambda R(\mathbf{f})$$

When $\lambda \to 0$, the approximation solution tends toward the interpolation solution. More elaborate approximation problems are sometimes useful, where for example

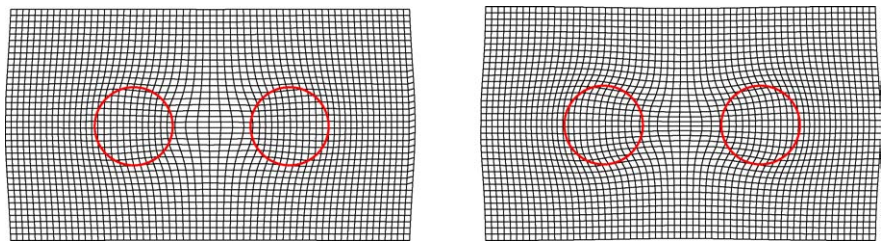

Figure 6. Two circles initially closed to each other are moved apart. Result of registration, using filters without (left) and with (right) cross-effects. Without cross-effects, horizontal lines stay horizontal outside the circles, and there is no noticeable vertical deformation. With cross-effects, the material between the circles is compressing vertically to compensate the horizontal dilatation.

the isotropic distance $\|\mathbf{g}_i - \mathbf{f}(\mathbf{x}_i)\|^2$ is replaced by an anisotropic distance depending on the index i [20].

4.2. *Vectorial Laplacian Splines*

For vector interpolation and approximation, the most common solution in the field of non-rigid registration consists in interpolating or approximating every component independently with isotropic scalar kernel, such as Laplacian splines or radial basis functions. A notable exception is the elastic body spline of Davis et al. [8], which is based on linear elasticity. Unfortunately, the exact interpolation kernel of linear elasticity is ill-defined as it tends toward infinity at its center. Therefore, there is a need of higher-order splines having tunable cross-effects.

For vector interpolation or approximation problems, we propose to generalize Laplacian splines using the IDQFs given by (for simplicity, we drop one of the two energy parameters of Eq. (6) since splines are defined up to a global multiplicative coefficient):

$$E_n(\mathbf{f}) = \partial_{i_1 \ldots i_n}\mathbf{f}_{i_{n+1}}\partial_{i_1 \ldots i_n}\mathbf{f}_{i_{n+1}} + \kappa\,\partial_{i_1 i_2 \ldots i_n}\mathbf{f}_{i_{n+1}}\partial_{i_{n+1} i_2 \ldots i_n}\mathbf{f}_{i_1}$$

As for the scalar case [10], if $n > d/2$, we note S_n the solution of

$$(-1)^n[\Delta^n S_n + \kappa\Delta^{n-1}\nabla\nabla^T S_n] = \delta\mathrm{Id} \qquad (10)$$

then the solution $\mathbf{f}$ of the vector interpolation or approximation problem has the following form

$$\mathbf{f}(\mathbf{x}) = \mathbf{p}(\mathbf{x}) + \sum_i S_n(\mathbf{x} - \mathbf{x}_i)\boldsymbol{\alpha}_i \qquad (11)$$

where $\mathbf{p}$ is a polynomial such that $E_n(\mathbf{p}) = 0$, and $\boldsymbol{\alpha}_i \in \mathbb{R}^d$ are coefficients that can be found by solving a set of linear equations.

4.2.1. Closed-Form Formulas. As in the scalar case, it is possible to get closed-form formulas for S_n. Getting into the Fourier domain, the PDE (10) becomes

$$[(\mathbf{w}^T\mathbf{w})^n\mathrm{Id} + \kappa(\mathbf{w}^T\mathbf{w})^{n-1}\mathbf{w}\mathbf{w}^T]\hat{S}_n = \mathrm{Id}$$

and we find that

$$\hat{S}_n = \frac{1}{(\mathbf{w}^T\mathbf{w})^n}\mathrm{Id} - \frac{\kappa}{(1+\kappa)(\mathbf{w}^T\mathbf{w})^{n+1}}\mathbf{w}\mathbf{w}^T$$

The Fourier transform of the scalar Laplacian spline s_n is precisely $\frac{1}{(\mathbf{w}^T\mathbf{w})^n}$. Thus, we can express S_n as a function of s_n and s_{n+1}:

$$S_n = s_n\mathrm{Id} + \frac{\kappa}{1+\kappa}\mathcal{H}s_{n+1}$$

where $\mathcal{H}s_{n+1}$ is the Hessian matrix of s_{n+1}.

4.2.2. Example: Vectorial Thin Plate Spline Interpolation. Up to a multiplicative coefficient, the 2-D second order Laplacian spline (or thin plate spline) is $s_2(x, y) = r^2 \ln r^2$, and the 2-D third-order Laplacian spline is $s_3(x, y) = r^4 \ln r^2$ [10], where $r^2 = x^2 + y^2$. One can thus calculate $\mathcal{H}s_3$, and find the close form formula of S_2 in 2D: $(S_2)_{1,1} = r^2 \ln r^2 + \frac{\kappa}{1+\kappa}[2(3x^2 + y^2)\ln r^2 + 7x^2 + y^2]$, $(S_2)_{1,2} = 2\frac{\kappa}{1+\kappa}xy(2\ln r^2 + 3)$.

In Fig. 7, we compare the results of the interpolation of displacement using scalar and vectorial thin plate splines. In the original position, the four points were placed at each corner of a square. The upper point has then been forced to move to the center of the square. The scalar thin-plate spline interpolation applied on each component independently, Fig. 7(a), does not present any horizontal displacement, and thus vertical lines remain straight. It possesses a strong accumulation of matter just under the point that has been moved. The vectorial Laplacian spline interpolation, Fig. 7(b), is more realistic thanks to a better distribution of the resulting displacements into both vertical and horizontal components; the previous accumulation of matter has disappear.

5. Merging Filters and Splines

In this section, we merge the two previous problems of dense (Section 3) and sparse (Section 4) vector approximation: we are searching for a vector field $\mathbf{f} : \mathbb{R}^d \to \mathbb{R}^d$ that approximates both a dense vector field $\mathbf{g}_1$, and a set of discrete pairings $\mathbf{g}_2$. The energy to minimize is

$$E(\mathbf{f}) = \int \|\mathbf{f} - \mathbf{g}_1\|^2 + \gamma \sum_{i=1\ldots p} \|\mathbf{f}(\mathbf{x}_i) - \mathbf{g}_2(\mathbf{x}_i)\|^2 + R(\mathbf{f}) \qquad (12)$$

It is shown in Appendix B that the optimal solution $\mathbf{f}$ is a linear combination of a smoothed vector field and

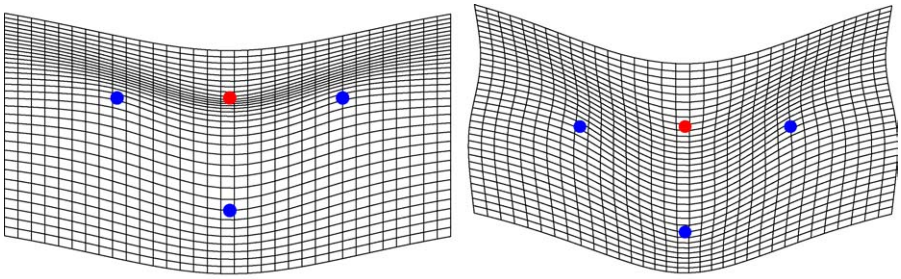

Figure 7. Interpolation of displacement using splines. One of four points initially forming a square is forced to move downwards. Without cross effects, vertical lines remain vertical and straight, and the material present a strong accumulation of matter in front of the translated point. When using cross-effects, the displacement field involves both vertical and horizontal components, producing a more realistic result.

a sum of splines

$$\mathbf{f}(\mathbf{x}) = K * \mathbf{g}_1(\mathbf{x}) + \sum_i K(\mathbf{x} - \mathbf{x}_i)\boldsymbol{\alpha}_i \qquad (13)$$

where K is the smoothing kernel associated to R, as those found in Section 3, and $\boldsymbol{\alpha}_i \in \mathbb{R}^d$ are coefficients found by solving a set of linear equations. Note that the same kernel is used both as a smoothing kernel to smooth C_1, and as a spline to approximate the sparse correspondences C_2. Contrary to the vectorial Laplacian splines of Section 4.2, these splines are bounded and decrease towards zero at infinity.

This formulation turns out to be very useful in the context of non-rigid registration, when one wants to add sparse geometric constraints to an intensity based algorithm, because the intensity similarity measure gives dense pairings $\mathbf{g}_1$, while geometric constraint gives sparse pairings $\mathbf{g}_2$.

We successfully applied this technique to the difficult problem of intersubject brain registration [6]. Because of the high variability of the cortex topology between different subjects, it is difficult to obtain valid registration results using the intensity alone. On the other hand, geometric features provided for instance by a set of sulcal lines extracted on the cortex, are too sparse to provide a dense and accurate non-rigid registration field everywhere. The idea developed in [6] is to combine intensity-based and feature-based registration with the above presented technique. The geometric features correspond to a set of sulcal lines automatically labeled by the Rivière-Mangin et al. algorithm [19], which we added to the `PASHA` registration scheme, presented in [5]. We present one of these results, because we believe it provides a nice illustration of the concepts developed in this article on a set of real images.

We show in Figs. 8(a) and (b) the position of 3 important cortical sulci extracted from the images of 5 different brains resp. before non-rigid registration (i.e. only a global affine alignment is applied to each brain with a reference one) and after. An important parameter is γ which allows the user to adjust the influence of feature-based pairings on the deformation field. One can see that it is possible to obtain a good geometric correspondence while preserving a smooth and one-to-one deformation field (Fig. 8(c)).

6. Conclusion

In this paper we introduced some new techniques for regularizing vector fields. We first studied isotropic quadratic energies, and then used these energies to deduce vector filters and splines to approximate respectively dense and sparse vector fields. We also introduced a separable vector filter that generalizes Gaussian filtering to vectors and enables a particularly efficient smoothing, using recursive filtering. Finally, we combined both sparse and dense approximation problems, and showed that the interesting closed-form solution can be applied successfully to real problems.

The original feature of vector regularization is the possibility to have cross-effects between coordinates, which is not possible using standard scalar regularization on each component separately. This new parameter makes it possible to more finely tune the solution of our problem, in the context of non-rigid registration for example, depending on our prior knowledge. Future quantitative analysis should demonstrate improvement of the motion recovery using the models proposed in this paper depending on the nature of the deformed material.

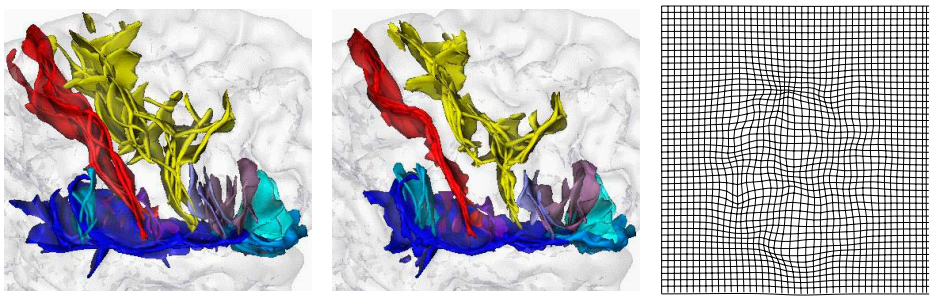

a. Before registration b. After registration c. Deformation sample

Figure 8. Results of interpatient brain registration based on intensity and geometric features, using Eq. (12) for regularization. Bright, medium and dark ribbons correspond resp. to precentral, central and temporal sulci of the 5 brains used in this registration experiment. Our registration scheme enables to strongly reduce the interindividual sulcal variability while keeping estimated transformations smooth and one-to-one, as shown on the right on one of the transformations. Images published originally in [5].

Appendix

A. *Reduction of Second Order IDQF Generators*

According to Theorem 1, the 15 quadratic forms that generate the set of second order IDQFs are

$$\begin{array}{lll}
\partial_{ii} f_j \partial_{jk} f_k \ (14) & \partial_{ii} f_j \partial_{kj} f_k \ (19) & \partial_{ii} f_j \partial_{kk} f_j \ (24) \\
\partial_{ij} f_i \partial_{jk} f_k \ (15) & \partial_{ij} f_i \partial_{kj} f_k \ (20) & \partial_{ij} f_i \partial_{kk} f_j \ (24) \\
\partial_{ij} f_j \partial_{ik} f_k \ (16) & \partial_{ij} f_k \partial_{ij} f_k \ (21) & \partial_{ij} f_k \partial_{ik} f_j \ (25) \\
\partial_{ij} f_j \partial_{ki} f_k \ (17) & \partial_{ij} f_k \partial_{ji} f_k \ (22) & \partial_{ij} f_k \partial_{ki} f_j \ (26) \\
\partial_{ij} f_j \partial_{kk} f_i \ (18) & \partial_{ij} f_k \partial_{jk} f_i \ (23) & \partial_{ij} f_k \partial_{kj} f_i \ (27)
\end{array}$$

Because we suppose that the derivation commutes with itself, some of these 15 quadratic forms are equal. It is straightforward to see that (14) = (19), (15) = (20), (16) = (17), (21) = (22), (23) = (28) and (26) = (27). Renaming $i \to j$ and $j \to i$, we also find (16) = (20), (18) = (25) and (26) = (28). We now have only 6 quadratic forms:

$$\begin{array}{lll}
\partial_{ij} f_j \partial_{ik} f_k \ (29) & \partial_{ij} f_k \partial_{ij} f_k \ (31) & \partial_{ij} f_i \partial_{kk} f_j \ (33) \\
\partial_{ii} f_j \partial_{kj} f_k \ (30) & \partial_{ii} f_j \partial_{kk} f_j \ (32) & \partial_{ij} f_k \partial_{kj} f_i \ (34)
\end{array}$$

Now, because the multiplication commutes, two of these 6 quadratic forms are also equal. Renaming $k \to i$ and $i \to k$, we see that (30) = (33). We finally have only 5 independent quadratic forms:

$$\partial_{ij} f_j \partial_{ik} f_k \quad \partial_{ii} f_j \partial_{kj} f_k \quad \partial_{ij} f_k \partial_{ij} f_k \quad \partial_{ii} f_j \partial_{kk} f_j \quad \partial_{ij} f_k \partial_{kj} f_i$$

B. *Sparse-and-Dense Approximation*

For sparse and dense approximation, we minimize the energy (12), which we first rewrite in the Fourier domain:

$$E(\mathbf{f}) = \int \|\hat{\mathbf{f}} - \hat{\mathbf{g}}_1\|^2 + \gamma \sum_{i=1\ldots p} \|\mathbf{f}(\mathbf{x}_i) - \mathbf{g}_2(\mathbf{x}_i)\|^2 + \int P(\mathbf{w}) \cdot \|\hat{\mathbf{f}}\|^2$$

where $P(\mathbf{w})$ is a polynomial matrix related to the IDQF R, and which is a linear combination of the terms $\lambda(\mathbf{w}^T\mathbf{w})^n + \lambda\kappa(\mathbf{w}^T\mathbf{w})^{n-1}\mathbf{w}\mathbf{w}^T$ if R is on the form (8). Since $\mathbf{f}(\mathbf{x}_i) = \int \hat{\mathbf{f}}(\mathbf{w}) \exp(2\pi i \cdot \mathbf{w}^T\mathbf{x}_i)$, the formal differentiation of this energy w.r.t. $\hat{\mathbf{f}}$ leads to

$$(\hat{\mathbf{f}} - \hat{\mathbf{g}}_1) + \gamma \sum_{i=1\ldots p} (\mathbf{f}(\mathbf{x}_i) - \mathbf{g}_2(\mathbf{x}_i)) \exp(-2\pi i \mathbf{w}^T\mathbf{x}_i) + P(\mathbf{w}) \cdot \hat{\mathbf{f}} = 0$$

The solution of this equation is

$$\hat{\mathbf{f}} = M^{-1}\hat{\mathbf{g}}_1 + \gamma \sum_{i=1\ldots p} \exp(-2\pi i \mathbf{w}^T\mathbf{x}_i) M^{-1} \times (\mathbf{g}_2(\mathbf{x}_i) - \mathbf{f}(\mathbf{x}_i))$$

where M^{-1} is the invert matrix of $M = \mathrm{Id} + P(\mathbf{w})$, with the same notation of Section 3.3.2.

Let us note K the inverse Fourier transform of M^{-1}. In the real domain, the first term $M^{-1}\hat{\mathbf{g}}_1$ transforms as $K * \mathbf{g}_1$, as in Section 3. Furthermore, $\exp(-2\pi i \mathbf{w}^T\mathbf{x}_i)M^{-1}$ is the Fourier transform of $K(\mathbf{x} - \mathbf{x}_i)$, so the second term transforms as

$\gamma \sum_i K(\mathbf{x} - \mathbf{x}_i)(\mathbf{g}_2(\mathbf{x}_i) - \mathbf{f}(\mathbf{x}_i))$. The solution to this approximation problem is thus of the form

$$\mathbf{f}(\mathbf{x}) = K * \mathbf{g}_1(\mathbf{x}) + \sum_{i=1\ldots p} K(\mathbf{x} - \mathbf{x}_i)\boldsymbol{\alpha}_i$$

where $\boldsymbol{\alpha}_i = \gamma(\mathbf{g}_2(\mathbf{x}_i) - \mathbf{f}(\mathbf{x}_i)) \in \mathbb{R}^d$ is a set of multiplicative coefficient that solve the set of equation:

$$K * \mathbf{g}_1(\mathbf{x}_i) + \sum_j K(\mathbf{x}_i - \mathbf{x}_j)\boldsymbol{\alpha}_j = \mathbf{g}_2(\mathbf{x}_i) - \boldsymbol{\alpha}_i/\gamma \qquad \forall i \in [\![1; p]\!]$$

This linear system can be rewritten as

$$\left(\frac{1}{\gamma}\mathrm{Id} + W\right)\boldsymbol{\alpha} = \boldsymbol{\beta}$$

with $\boldsymbol{\alpha}$ being the vector of size pd of all the coefficient

$$\boldsymbol{\alpha} = \left(\boldsymbol{\alpha}_1^T, \ldots, \boldsymbol{\alpha}_p^T\right)^T$$

W the $pd \times pd$ matrix

$$W = (K(\mathbf{x}_i - \mathbf{x}_j)) = \begin{pmatrix} K(\mathbf{x}_1 - \mathbf{x}_1) & K(\mathbf{x}_1 - \mathbf{x}_2) & \cdots & K(\mathbf{x}_1 - \mathbf{x}_p) \\ K(\mathbf{x}_2 - \mathbf{x}_1) & \ddots & & \vdots \\ \vdots & & \ddots & \vdots \\ K(\mathbf{x}_p - \mathbf{x}_1) & \cdots & \cdots & K(\mathbf{x}_p - \mathbf{x}_p) \end{pmatrix}$$

and $\boldsymbol{\beta}$ the vector of size pd

$$\boldsymbol{\beta} = ((\mathbf{g}_2(\mathbf{x}_1) - K * \mathbf{g}_1(\mathbf{x}_1))^T, \ldots, (\mathbf{g}_2(\mathbf{x}_p) - K * \mathbf{g}_1(\mathbf{x}_p))^T$$

Acknowledgments

The authors wish to thank Jean-François Mangin and his group for providing the datasets on automatically labelled cortical sulci and the visualization software used for the experiments described in Section 5 and Fig. 8.

Note

1. Here, we will not distinguish between covariant and contravariant coordinates.

References

1. L. Alvarez, J. Weickert, and J. Sánchez, "Reliable estimation of dense optical flow fields with large displacements," *Int. J. of Comp. Vision*, Vol. 39, No. 1, pp. 41–56, 2000.
2. R. Bajcsy and S. Kovačič, "Multiresolution elastic matching," *Comp. Vision, Graphics and Image Processing*, Vol. 46, pp. 1–21, 1989.
3. P. Blomgren and T.F. Chan, "Color tv: Total variation methods for restoration of vector valued images," *IEEE Trans. Image Proc.*, Vol. 7, No. 3, pp. 304–309, 1996.
4. M. Brady and B.K.P. Horn, "Rotationally symmetric operators for surface interpolation," *Comp. Vision, Graphics, and Image Processing*, Vol. 22, pp. 70–94, 1983.
5. P. Cachier, E. Bardinet, D. Dormont, X. Pennec, and N. Ayache, "Iconic feature based nonrigid registration: The PASHA algorithm," *Comp. Vision and Image Underst.*, Vol. 89, Nos. 2/3, pp. 272–298, 2003.
6. P. Cachier, J.-F. Mangin, X. Pennec, D. Rivière, D. Papadopoulos-Orfanos, J. Régis, and N. Ayache, "Multisubject non-rigid registration of brain MRI using intensity and geometric features," in *Proc. of MICCAI'01*, Vol. 2208 of *LNCS*, Utrecht, the Netherlands, 2001, pp. 734–742.
7. V. Casalles, G. Sapiro, and D.-H. Chung, "Vector median filters, inf-sup operations, and coupled PDE's: Theoretical connections," *J. Math. Imaging and Vision*, Vol. 8, pp. 109–119, 2000.
8. M.H. Davis, A. Khotanzad, D.P. Flamig, and S.E. Harms, "A physics-based coordinate transformation for 3D image matching," *IEEE Trans. on Medical Imaging*, Vol. 16, No. 3, pp. 317–328, 1997.
9. R. Deriche, "Recursively implementing the Gaussian and its derivatives," in *2nd Int. Conf. on Image Processing*, 1992, pp. 263–267.
10. J. Duchon, "Interpolation des fonctions de deux variables suivant le principe de la flexion des plaques minces," *RAIRO Analyse Numérique*, Vol. 10, No. 12, pp. 5–12, 1976.
11. M. Gabrani, "Multidimensional spline interpolation theory and surface-based alignment of brains," PhD thesis, Drexel University, Philadelphia, USA, 1998.
12. P. Hellier, C. Barillot, E. Mémin, and P. Pérez, "Medical image registration with robust multigrid techniques," in *Proc. of MICCAI'99*, Vol. 1679 of *LNCS*, Cambridge, UK: Springer, 1999, pp. 680–687.
13. H. Jeffreys, "On isotropic tensors," *Proc. of Cambridge Phil. Soc.*, Vol. 73, pp. 173–176, 1973.
14. P. Kannappan and P.K. Sahoo, "Rotation invariant separable functions are Gaussian," *SIAM J. on Math. Analysis*, Vol. 23, No. 5, pp. 1342–1351, 1992.
15. R. Kimmel, R. Malladi, and N. Sochen, "Images as embedded maps and minimal surfaces: Movies, color, texture, and volumetric medical images," *Int. J. Comp. Vision*, Vol. 39, No. 2, pp. 111–129, 2000.
16. R. Lakes, "Foam structures with a negative Poisson's ratio," *Science*, Vol. 235, No. 4792, pp. 1038–1040, 1987.
17. M. Nielsen, L. Florack, and R. Deriche, "Regularization and scale space," Research Report RR-2352, INRIA, 1994.
18. D. Rey, G. Subsol, H. Delingette, and N. Ayache, "Automatic detection and segmentation of evolving processes in 3D medical images: Application to multiple sclerosis," in *Proc. of*

IPMI'99, Vol. 1613 of *LNCS*, Visegrad, Hungary, 1999, pp. 154–167.
19. D. Rivière, J.-F. Mangin, D. Papadopoulos, J.-M. Martinez, V. Frouin, and J. Régis, "Automatic recognition of cortical sulci using a congregation of neural networks," in *Proc. of MICCAI'00*, Vol. 1935 of *LNCS*, Pittsburgh, USA: Springer, 2000, pp. 40–49.
20. K. Rohr, M. Fornefett, and H.S. Stiehl, "Approximating thin-plate splines for elastic registration: Integration of landmark errors and orientation attributes," in *Proc. of IPMI'99*, Vol. 1613 of *LNCS*, Visegrád, Hungary: Springer, 1999, pp. 252–265.
21. G. Sapiro and D.L. Ringach, "Anisotropic diffusion of multivalued images with applications to color filtering," *IEEE Trans. Image Proc.*, Vol. 5, No. 11, pp. 1582–1586, 1996.
22. G.F. Smith, "On isotropic tensors and rotation tensors of dimension *m* and order *n*," *Tensor, N. S.*, Vol. 19, pp. 79–88, 1968.
23. R. Szeliski, "Bayesian modeling of uncertainty in low-level vision," *Int. J. of Comp. Vision*, Vol. 5, No. 3, pp. 271–301, 1990.
24. D. Terzopoulos, "Regularization of inverse visual problems involving discontinuities," *IEEE Trans. on Pattern Analysis and Machine Intelligence*, Vol. 8, No. 4, pp. 413–424, 1986.
25. A. Tsai, A. Yezzi, and A.S. Willsky, "A curve evolution approach to medical image magnification via the Mumford-Shah functional," in *Proc. of MICCAI'00*, Vol. 1935 of *LNCS*, Pittsburgh, USA: Springer, 2000, pp. 246–255.
26. H. Weyl, *The Classical Groups: Their Invariants and Representations*, Princeton University Press, 1966.

Pascal Cachier received his M.S. on Artificial Intelligence and Image Processing from the Ecole Normale Superieure de Cachan in 1998, and his Ph.D. from the Ecole Centrale Paris in 2002 on topics related to Medical Image Registration, under the supervision of Pr. Nicholas Ayache. After graduation, he spent one year at the International University in Germany, under the supervision of Pr. Karl Rohr, teaching and working on intensity and landmark based registration. Pascal Cachier is now with the CAD group at Siemens Medical Solutions USA, Inc. His research interests include Computer-Aided Diagnosis, Segmentation, and Registration.

Nicholas Ayache is a Research Director at INRIA (French Research Institute in Computer Science and Automatic Control), Sophia-Antipolis, France, where he has been the scientific leader of the EPIDAURE research group on medical image analysis and robotics since 1993. He is also teaching graduate courses in computer vision at the Universities of Nice-Sophia-Antipolis and Paris XI and also at Ecole Centrale Paris. During the past 15 years, he has been a scientific consultant for several industrial companies.

Dr. Ayache received his Ph.D in 1983, and his "Thèse d'Etat" in 1988, both in computer science, from the University of Paris XI, on topics related to model based object recognition, passive stereovision, and multisensor fusion. His current research interests are medical image processing and analysis, (including shape and motion representation, rigid and nonrigid registration, tracking and analysis of deformable objects), simulation of surgery (including the modelling of soft tissue), and image guided therapy (in particular in the context of medical robotics). He is also involved in the analysis of functional images and their application to medicine and neurosciences. He is the author and co-author of numerous scientific publications in these domains.